

Derivation of CPT resonance signals from density-matrix equations with all relevant sublevels of Cs atoms and confirmation of experimental results

Kenta Matsumoto^{1,2}, Sota Kagami^{1,2}, Takahiro Fujisaku^{1,2}, and Akihiro Kiriwara^{1,2}

¹Secure System Platform Research Laboratories, NEC Corporation, 1753 Shimonumabe, Nakahara-ku, Kawasaki, Kanagawa 211-0011, Japan

²National Institute of Advanced Industrial Science and Technology (AIST), NEC-AIST Quantum Technology Cooperative Research Laboratory, 1-1-1 Umezono, Tsukuba, Ibaraki 305-8568, Japan

Shinya Yanagimachi³

³National Institute of Advanced Industrial Science and Technology (AIST), 1-1-1 Umezono, Tsukuba, Ibaraki 305-8563, Japan

Takeshi Ikegami⁴ and Atsuo Morinaga⁴

⁴Micromachine Center, AIST Tsukuba East 4G, 1-2-1 Namiki, Tsukuba, Ibaraki 305-8564, Japan

(Abstract)

Coherent-population-trapping resonance is a quantum interference effect that appears in the two-photon transitions between the ground-state hyperfine levels of alkali atoms and is often utilized in miniature clock devices. To quantitatively understand and predict the performance of this phenomenon, it is necessary to consider the transitions and relaxations between all hyperfine Zeeman sublevels involved in the different excitation processes of the atom. In this study, we constructed a computational multi-level atomic model of the Liouville density-matrix equation for 32 Zeeman sublevels involved in the D_1 line of ^{133}Cs irradiated by two frequencies with circularly polarized components and then simulated the amplitude and shape of the transmitted light through a Cs vapor cell. We show that the numerical solutions of the equation and analytical investigations adequately explain a variety of the characteristics observed in the experiment.

I. INTRODUCTION

Coherent-population-trapping (CPT) resonance is a quantum interference phenomenon observed using a two-photon Λ -type transition between the ground hyperfine Zeeman sublevels of an alkali atom [1,2]. Thanks to its high Q factor at the microwave transition [3], it is currently utilized as a key spectroscopic technique for creating miniature atomic clock devices. In more than 20 years following the first detection of CPT resonance in vapor cells [4,5] and proposal for microfabricated atom vapor cells [6-8], ongoing advancements have led to the development of miniature atomic clocks using silicon micromachining and semiconductor laser technology [9], the achievement of high contrast signal [10], and increased robustness of the resonance frequency to fluctuations in the external environment and the excitation light itself [11,12].

The optical excitation scheme originally utilized in the CPT clock featured a circular polarization for bichromatic

excitation lights, $\sigma^- - \sigma^-$ or $\sigma^+ - \sigma^+$, but such polarization pumps a significant fraction of the atoms into Zeeman edge (trap) states, thus reducing the contrast of the CPT signal. To prevent this reduction, excitation schemes such as push-pull optical pumping [13], counter-propagating $\sigma^+ - \sigma^-$ polarization [14], a pair of orthogonal linear polarizations (Lin \perp Lin) [15], or a pair of parallel linear polarizations (Lin \parallel Lin) [16] have been proposed. The first three methods produce the CPT resonance between two hyperfine states $|F_g = 3, m = 0\rangle$ and $|F_e = 4, m = 0\rangle$ on each leg of the Λ scheme, namely (0, 0) CPT resonance [17]. This resonance is essentially a double- Λ scheme, in which a dark state common to the two Λ schemes exists [18]. In contrast, no (0, 0) CPT resonance occurs in the fourth method because the dark state for one Λ scheme is the bright state for the other. Instead, two CPT resonances are produced between $|F_g, m = -1\rangle$ and $|F_e, m = 1\rangle$ and between $|F_g, m = 1\rangle$ and $|F_e, m = -1\rangle$, namely (-1, 1) and (1, -1) CPT resonances. These doublet resonances split in frequency due to the second order Zeeman effect [19]. The relationship between the CPT resonance and excitation polarization scheme on ^{133}Cs atoms has been studied by Liu et al. [17].

In our previous work [20], we showed that the amplitudes of the (-1, 1) and (1, -1) CPT resonances excited with Lin \parallel Lin polarization increase approximately in proportion to the excitation intensity, while in contrast, the amplitude of the (0, 0) CPT resonance excited with $\sigma^- - \sigma^-$ polarization moderately saturates. We claimed that the former is best described by a simple three-level model and the latter by a four-level model with a trap state. However, a model that includes Zeeman sublevels, an extension of the three-level model for the Λ -type transition, is effective in quantitatively understanding of the amplitude of the CPT resonances. Furthermore, Taichenachev et al. reported that changes in the symmetry, linewidth, and frequency shift of the resonance spectrum are related to the optical detuning of the excitation lights [21]. These behaviors of the CPT spectrum can be better understood by solving the Liouville density-matrix equation taking into account 32 Zeeman sublevels related to the D_1 line of ^{133}Cs .

When constructing a model with 32 Zeeman sublevels, it is necessary to configure a detailed relaxation process between 16 ground levels, which is simple in the three-level model because there are only two ground levels. In 2017, Warren et al. developed an atomic model using the Liouville density-matrix equation taking into account all relevant 16 Zeeman sublevels in the D_1 line of ^{87}Rb atoms and compared the calculated results with the corresponding experimental results for excitation with three different polarization configurations [22]. They assumed a uniform relaxation process between the magnetic sublevels of the ground states. In an alternative approach, Matsuda et al. utilized the magnetic dipole relaxation between the magnetic sublevels of the ground states in the D_1 line of ^{133}Cs atoms [23].

We make two key contributions in the current work. First, we construct a multi-level atomic model of the Liouville density-matrix equation [24] for studying CPT resonances formed by the bichromatic lights of various excitation schemes in the manifold of ^{133}Cs atoms. Second, we simulate the amplitude and shape of the CPT resonance excited by different polarizations, frequencies, and intensities of the excitation lights, and elucidate the underlying mechanisms by comparing them with the corresponding experimental results. In Sec. II.A, we derive the

multi-level atomic model using the density matrix equation, and in II.B, we show the formulations for the line shape, linewidth, and light shift of the CPT resonance spectrum guided from the present multi-level atomic model. Section III describes our experimental setup and Cs vapor cells with buffer gas. In Sec. IV, we compare the experimental results with the calculated results. IV.A reports how the Zeeman CPT spectra with different buffer gas pressures vary due to the relaxation process. IV.B shows that the amplitude of the first order Zeeman CPT spectra depends on the common detuning frequency of the excitation light. In IV.C, we clarify that the (m, m) CPT resonance appears for $\text{Lin} \parallel \text{Lin}$ excitation (except for $(0, 0)$) in the second order Zeeman CPT spectrum and discuss the required conditions to prohibit the CPT resonances of double- Λ schemes. IV.D explains how the amplitude of the CPT resonance for $\sigma^- - \sigma^-$ excitation saturates while that for $\text{Lin} \parallel \text{Lin}$ excitation increases in proportion to the excitation intensity depending on the variation of the population in the trap state. We conclude in Sec. V with a brief summary. Appendix provides additional detail on how the shape of the CPT spectrum is rigorously derived from the 32-level model we utilized.

II. FORMULATION AND CALCULATION

A. Liouville equations for CPT spectrum

We aim to construct a multi-level atomic model including all the Zeeman sublevels in the D_1 transition of ^{133}Cs so as to theoretically investigate the CPT resonances excited with various polarizations. Figure 1 shows the energy structure of the hyperfine Zeeman sublevels in the D_1 line of ^{133}Cs under a magnetic field as a perturbation together with the definition of the energy detuning of the bichromatic excitation lights for the CPT resonance, whose angular frequencies are ω_1 and ω_2 . Though out this paper, all quantities of the energy detuning and energy levels are given in the unit of angular frequency. There are 32 Zeeman sublevels in the hyperfine ground states, $6\text{S}_{1/2} F=3$ and $F=4$, and in the hyperfine excited states, $6\text{P}_{1/2} F'=3$ and $F'=4$, some of which are coupled by the D_1 transition depending on the polarization of excitation lights. As shown in Fig. 1, Zeeman sublevels are designated from 1 to 32 in order of the magnetic quantum numbers m_F from $-F$ to F . We also designate sublevels belonging to $6\text{S}_{1/2} F=3$, $F=4$, and $6\text{P}_{1/2} F'=3$ or $F'=4$ as g , e , and i , respectively. The unperturbed energies of the hyperfine ground states, $6\text{S}_{1/2} F=3$ and $F=4$, are represented as ω_g^0 and ω_e^0 , respectively. ω_{i0} is the mean energy between the unperturbed energies of $6\text{P}_{1/2} F'=3$ and $F'=4$. The quantized magnetic field with strength B is applied along the direction of light propagation. We define energies of the Zeeman sublevels under the magnetic field B as ω_g^B , ω_e^B and ω_i^B , which are shifted by the Zeeman effect according to Breit-Rabi's formula [19].

The two photons ω_1 and ω_2 ($< \omega_1$) induce a three-level Λ -type CPT resonance between the two hyperfine levels in the ground state and an excited level. The energy detuning of ω_1 from the related D_1 transition energy is $\Delta_1 = \omega_1 - (\omega_{i0} - \omega_g^0)$. Similarly, that of ω_2 is $\Delta_2 = \omega_2 - (\omega_{i0} - \omega_e^0)$. The Raman detuning of $\omega_1 - \omega_2$ from the

ground hyperfine splitting $(\Delta_{\text{hfs}} = \omega_e^0 - \omega_g^0)$ is given by $\Delta_R = (\omega_1 - \omega_2) - \Delta_{\text{hfs}}$. In the CPT resonance experiment, generally, the $+1^{\text{st}}$ and -1^{st} sidebands generated from a single laser source by modulating at a frequency of $(\Delta_{\text{hfs}} + \Delta_R)/2$ are used as the two photons ω_1 and ω_2 . As shown in Fig. 1, we define the common detuning Δ_{opt} as $\Delta_{\text{opt}} = \Delta_1 - \frac{\Delta_R}{2} = \Delta_2 + \frac{\Delta_R}{2}$.

The system with a set of the orthonormal quantum states $|1\rangle - |32\rangle$ corresponding to the 32 magnetic sublevels of a Cs atom (presented in Fig. 1) is described by the Heisenberg equation of the density matrix component ρ and the interaction Hamiltonian \mathcal{H} , as

$$\frac{\partial}{\partial t} \rho = \frac{1}{i\hbar} [\mathcal{H}, \rho] \quad (1)$$

where \hbar is the Planck constant divided by 2π . The coupling of the atomic states to two coherent radiation fields is described within the rotating wave approximation, as

$$\frac{1}{\hbar} \mathcal{H} = \sum_{l=1}^{32} \delta_l |l\rangle \langle l| - \frac{1}{2} \sum_{s=1}^{16} \sum_{t=17}^{32} (\Omega_{st} |s\rangle \langle t| + \Omega_{st}^* |t\rangle \langle s|) \quad (2)$$

where

$$\delta_l = \begin{cases} \omega_l^B - \omega_g^0 + \frac{\Delta_R}{2} & l = 1, \dots, 7 \\ \omega_l^B - \omega_e^0 - \frac{\Delta_R}{2} & l = 8, \dots, 16 \\ \omega_l^B - \omega_{l0} - \Delta_{\text{opt}} & l = 17, \dots, 32 \end{cases} \quad (3)$$

Here, the coupling term $\Omega_{st} = \langle s | (-\mathbf{d} \cdot \mathbf{E}) / \hbar | t \rangle = \Omega_{ts}^*$ is the Rabi frequency, where \mathbf{d} is the electric dipole moment and \mathbf{E} is the electric field of the excitation lights.

First, as the excitation light we consider a circularly polarized σ^+ light with the amplitude of $\mathcal{E}(t)$, which propagates along the z-axis. The Rabi frequency for σ^+ excitation light is defined as

$$\Omega_{st}^{\sigma^+} = -\frac{\mathcal{E}(t)}{\hbar} d_{FF'} \langle F', m'_F | F, 1, m_F, 1 \rangle. \quad (4)$$

Similarly, for a circularly polarized σ^- light, the Rabi frequency is defined as

$$\Omega_{st}^{\sigma^-} = -\frac{\mathcal{E}(t)}{\hbar} d_{FF'} \langle F', m'_F | F, 1, m_F, -1 \rangle. \quad (5)$$

Here, F and F' are the total angular momenta of $|s\rangle$ and $|t\rangle$, respectively. m_F and m'_F are the magnetic quantum numbers of $|s\rangle$ and $|t\rangle$, respectively. $d_{FF'}$ is the reduced matrix element of the dipole moment operator between levels whose total angular momenta are F and F' , and $\langle F', m'_F | F, 1, m_F, \pm 1 \rangle$ is the Clebsch-Gordan coefficient. These values for the Cs atom are given in [25].

Next, as the excitation light $\mathbf{E}(t)$, we consider the linearly polarized light with the amplitude of $\mathcal{E}(t)$ whose polarization forms an angle θ with the x-axis. The linearly polarized electric field is rewritten by the

superposition of two circular polarizations σ^+ and σ^- using the spherical vector basis $\mathbf{e}_{\pm l} = \mp(\mathbf{e}_x \pm i\mathbf{e}_y)/\sqrt{2}$, as

$$\mathbf{E}^{\text{lin}}(t, \theta) = \mathcal{E}(t)(\mathbf{e}_x \cos \theta + \mathbf{e}_y \sin \theta) = \frac{\mathcal{E}(t)}{\sqrt{2}}(-e^{-i\theta}\mathbf{e}_{+l} + e^{i\theta}\mathbf{e}_{-l}). \quad (6)$$

Using Eqs. (4) and (5), the Rabi frequency of the linear polarized light is rewritten as

$$\Omega_{st}^{\text{lin}} = -\frac{e^{-i\theta}}{\sqrt{2}}\Omega_{st}^{\sigma^+} + \frac{e^{i\theta}}{\sqrt{2}}\Omega_{st}^{\sigma^-}. \quad (7)$$

In the CPT resonance, the bichromatic excitation lights of ω_1 and ω_2 copropagating along z-axis interact with two ground hyperfine states and one excited state by a Λ -type scheme. The bichromatic Rabi frequency in this case is also composed of two Rabi frequencies $\Omega_{1st}(\mathcal{E}_1(t))$ and $\Omega_{2st}(\mathcal{E}_2(t))$, where $\mathcal{E}_1(t)$ and $\mathcal{E}_2(t)$ are the amplitudes of the excitation lights of ω_1 and ω_2 , respectively. Since the detuned frequency component disappears due to the rotating wave approximation, $\Omega_{2st}(\Omega_{1st})$ disappears for $s=1, \dots, 7$ ($8, \dots, 16$). Let us assume the direction of the electric field of ω_1 is parallel to the x-axis, while that of ω_2 forms an angle θ with the x-axis. The coupling term is then written as

$$\Omega_{st}^{\text{lin}} = \begin{cases} \Omega_{1st}^{\text{lin}} = -\frac{1}{\sqrt{2}}\Omega_{1st}^{\sigma^+} + \frac{1}{\sqrt{2}}\Omega_{1st}^{\sigma^-} & s=1, \dots, 7 \\ \Omega_{2st}^{\text{lin}} = -\frac{e^{-i\theta}}{\sqrt{2}}\Omega_{2st}^{\sigma^+} + \frac{e^{i\theta}}{\sqrt{2}}\Omega_{2st}^{\sigma^-} & s=8, \dots, 16 \end{cases}. \quad (8)$$

In the Lin \parallel Lin polarization scheme, we adopt $\Omega_{2st}^{\text{lin}}$ with $\theta=0$. In the Lin \perp Lin polarization scheme, which corresponds to the push-pull scheme, we adopt $\Omega_{2st}^{\text{lin}}$ with $\theta=\pi/2$.

The evolution of the atomic system is governed by the Liouville equation, namely, the equation of motion for the density operator $\hat{\rho} = \sum_{l=1}^{32} \sum_{m=1}^{32} \rho_{lm} |l\rangle\langle m|$, as follows.

$$\frac{\partial}{\partial t} \hat{\rho} = -\frac{i}{\hbar}(\hat{H}\hat{\rho} - \hat{\rho}\hat{H}) - \frac{i}{\hbar}(\hat{H}'_\Gamma \hat{\rho} + \hat{\rho}\hat{H}'_\Gamma) + \hat{\Lambda}, \quad (9)$$

where a non-Hermitian operator \hat{H}'_Γ and a source matrix $\hat{\Lambda}$ are added to reflect the relaxation process. \hat{H}'_Γ accounts for the decays of atomic states by defining

$$\frac{i}{\hbar}\hat{H}'_\Gamma = -\frac{i}{2}\sum_{l=1}^{32}\Gamma_l |l\rangle\langle l| = -\frac{i}{2}\left(\gamma_p \sum_{l=1}^{16} |l\rangle\langle l| + \Gamma \sum_{l=17}^{32} |l\rangle\langle l|\right), \quad (10)$$

where Γ_l is the total decay rate of a sublevel $|l\rangle$ and is a value that depends on several experimental parameters (e.g., the pressure of buffer gas, temperature, and the coating situation of the cell wall). For simplicity, we assume that all excited states have the same decay rate Γ , namely, $\Gamma_l = \Gamma$ for $l=17, \dots, 32$, which can be determined from the linewidth of the absorption spectrum. Similarly, those of all ground hyperfine states are assumed to be γ_p ,

namely, $\Gamma_l = \gamma_p$ for $l=1, \dots, 16$, which is estimated from the linewidth of the CPT spectrum.

On the other hand, the source matrix $\hat{\Lambda}$ contains non-zero diagonal elements that account for the influx of atoms decaying from other states, as follows:

$$\hat{\Lambda} = \sum_{l=1}^{32} \Lambda_l (\Gamma_1 \rho_{11}, \Gamma_2 \rho_{22}, \dots, \Gamma_{32} \rho_{3232}) |l\rangle \langle l|. \quad (11)$$

Λ_l represents the total influx rate of $|l\rangle$, which is a function of the product of decay rate Γ_m and the population ρ_{mm} of state $|m\rangle$. We ignore the influx rates into the excited states because these are by far smaller than those into the ground states; $\Lambda_l = 0$ for $l=17, \dots, 32$. We assume that the decay process from an excited state $|n\rangle$ to a ground state $|m\rangle$ is governed by cesium-nitrogen collisions, and the decay rates are proportional to the square of the normalized dipole matrix element [25], T_{nm}^2 , which satisfies $\sum_{m=1}^{16} T_{nm}^2 = 1$. As for the relaxation between magnetic sublevels of the ground states, we consider two different processes, depending on the experimental conditions. One is a uniform relaxation process [22] (illustrated in Fig. 2 (a)) that is caused by collisional relaxation between Cs atoms, collisional relaxation between Cs and wall surfaces, and the replacement of atoms in the optical path with those in thermal equilibrium outside the optical path. The source matrix for the uniform relaxation process $\Lambda_l^{(uni)}$ is written as

$$\Lambda_l^{(uni)} = \sum_{m=1, m \neq l}^{16} \frac{1}{15} \gamma_p^{(uni)} \rho_{mm} + \sum_{n=17}^{32} T_{nl}^2 \Gamma \rho_{nn} \text{ for } l=1, \dots, 16, \quad (12)$$

where $\gamma_p^{(uni)}$ is the decay rate of a ground state $|m\rangle$ for $m=1, \dots, 16$. The first and second terms represent the influxes from ground states other than itself and from the excited states, respectively. The other relaxation process is the magnetic dipole relaxation $\Lambda_l^{(M1)}$, whose transition distribution is proportional to the square of the Clebsch-Gordan coefficient [25],

$$\Lambda_l^{(M1)} = \sum_{m=1, m \neq l}^{16} \tilde{T}_{ml}^2 \gamma_p^{(M1)} \rho_{mm} + \sum_{n=17}^{32} T_{nl}^2 \Gamma \rho_{nn} \text{ for } l=1, \dots, 16. \quad (13)$$

Here, $\tilde{T}_{ml}^2 = T_{ml}^2 / (1 - T_{mm}^2)$, which satisfies $\sum_{l=1, l \neq m}^{16} \tilde{T}_{ml}^2 = 1$. It will be necessary to estimate how these processes contribute to the relaxation in the experimental system.

The Liouville equation (9) for each matrix element is written as

$$\frac{\partial}{\partial t} \rho_{lm} = \langle l | \frac{\partial}{\partial t} \hat{\rho} | m \rangle = - \left[\frac{\Gamma_l + \Gamma_m}{2} + i(\delta_l - \delta_m) \right] \rho_{lm} + \frac{i}{2} \sum_{u=1}^{32} (\Omega_{lu} \rho_{um} - \rho_{lu} \Omega_{um}) + \Lambda_l \delta_{lm}, \quad (14)$$

where δ_{lm} is Kronecker's symbol. These equations are rearranged as a vector matrix equation in the form $\frac{\partial}{\partial t} \mathbf{p} = M \mathbf{p}$, where \mathbf{p} is a vector consisting of 1024 elements ρ_{lm} and M is a (1024×1024) matrix consisting of the coefficients of ρ_{lm} generated from the right side of Eq. (13). We developed a computational program to calculate steady-state solutions for ρ_{lm} by equating $\frac{\partial}{\partial t} \mathbf{p}$ to zero using the condition $\sum_{m=1}^{32} \rho_{mm} = 1$ for a closed

atomic system. From Eqs. (10–13), Λ_l should be written to satisfy the population conservation, $\sum_{m=1}^{32} \frac{\partial}{\partial t} \rho_{mm} = 0$.

In this calculation of the Liouville equation with a multi-level model, we ignore other sideband lights except for the $\pm 1^{\text{st}}$ order sidebands, and we set $\mathcal{E}_1(t) = \mathcal{E}_2(t) = \mathcal{E}(t)/\sqrt{2}$ for simplicity. At the steady-state condition of Eq. (14), the population of an excited state $|n\rangle (n=17, \dots, 32)$, ρ_{nn} , is written as

$$\rho_{nn} = -\sum_{l=1}^{16} \frac{\text{Im}(\Omega_{nl} \rho_{ln})}{\Gamma_n}. \quad (15)$$

Then, the amplitude of the CPT resonance is determined as the variation between the sums of the populations of the excited states $\sum_{n=17}^{32} \rho_{nn}$ on resonance and off resonance.

B. Line shape, linewidth, and light shift

We reveal how the formulations for the line shape, linewidth, and light shift of the CPT resonance spectrum are guided from the present multi-level atomic model. Here, we assume that the lower ground level $|g\rangle (g=1, \dots, 7)$ and the upper ground level $|e\rangle (e=8, \dots, 16)$ constitute the CPT resonance. As a necessary condition for CPT resonance to be observed, there exists at least one excited level $|i\rangle (i=17, \dots, 32)$ such that the Rabi frequency determined by the given excitation light is $\Omega_{gi} \neq 0$ and $\Omega_{ei} \neq 0$. Substituting $l=g$, $m=e$ into Eq. (13), the

coherence ρ_{ge} excited between the ground-state sublevels, $|g\rangle$ and $|e\rangle$, can be written as

$$\left[\frac{\Gamma_g + \Gamma_e}{2} + i(\delta_g - \delta_e) \right] \rho_{ge} = \frac{i}{2} \sum_{u=17}^{32} (\Omega_{gu} \rho_{ue} - \Omega_{eu}^* \rho_{gu}). \quad (16)$$

Since $\Gamma_u = \Gamma \gg \Gamma_g$ or Γ_e for the excited levels $|u\rangle (u=17, \dots, 32)$, we define optical decoherence as $\gamma_f = \frac{\Gamma}{2}$

$\simeq \frac{\Gamma_u + \Gamma_g}{2} \simeq \frac{\Gamma_u + \Gamma_e}{2}$. ρ_{ue} and ρ_{gu} are then written as

$$\begin{aligned} \rho_{ue} &= \frac{i}{2} \frac{\Omega_{gu}^* \rho_{ge} + \sum_{s=1, s \neq g}^{16} \Omega_{su}^* \rho_{se} - \sum_{t=17}^{32} \Omega_{et}^* \rho_{ut}}{\gamma_f + i(\delta_u - \delta_e)}, \\ \rho_{gu} &= \frac{i}{2} \frac{-\Omega_{eu} \rho_{ge} + \sum_{t=17}^{32} \Omega_{gt} \rho_{tu} - \sum_{s=1, s \neq g}^{16} \Omega_{su} \rho_{gs}}{\gamma_f - i(\delta_u - \delta_g)}. \end{aligned} \quad (17)$$

We substitute these into the right-hand side of Eq. (16) and transfer the term containing ρ_{ge} to the left-hand side.

$$\rho_{ge} = \frac{-\frac{1}{4} \sum_{u=17}^{32} \left[\frac{\Omega_{gu} (\sum_{s=1, s \neq g}^{16} \Omega_{su}^* \rho_{se} - \sum_{t=17}^{32} \Omega_{et}^* \rho_{ut})}{\gamma_f + i(\delta_u - \delta_e)} + \frac{\Omega_{eu}^* (\sum_{s=1, s \neq g}^{16} \Omega_{su} \rho_{gs} - \sum_{t=17}^{32} \Omega_{gt} \rho_{tu})}{\gamma_f - i(\delta_u - \delta_g)} \right]}{\Delta_{\text{width}} + i(\delta_g - \delta_e - \Delta_{LS})} \quad (18)$$

$$\Delta_{width} = \frac{\Gamma_g + \Gamma_e}{2} + \frac{1}{4} \sum_{u=17}^{32} \left[\frac{|\Omega_{gu}|^2 \gamma_f}{\gamma_f^2 + (\delta_u - \delta_e)^2} + \frac{|\Omega_{ue}|^2 \gamma_f}{\gamma_f^2 + (\delta_u - \delta_g)^2} \right] \quad (19)$$

$$\Delta_{LS} = -\frac{1}{4} \sum_{u=17}^{32} \left[-\frac{|\Omega_{gu}|^2 (\delta_e - \delta_u)}{\gamma_f^2 + (\delta_u - \delta_e)^2} + \frac{|\Omega_{ue}|^2 (\delta_g - \delta_u)}{\gamma_f^2 + (\delta_u - \delta_g)^2} \right] \quad (20)$$

By replacing the numerator on the right side of Eq. (18) with \mathcal{C} , the relative part $\text{Re}(\rho_{ge})$, which determines the shape of the CPT resonance curve in the case where $\Omega_1 \Omega_2$ is a real value, becomes

$$\text{Re}(\rho_{ge}) = -\frac{\text{Re}(\mathcal{C}) \Delta_{width}}{\Delta_{width}^2 + (\delta_g - \delta_e - \Delta_{LS})^2} + \frac{\text{Im}(\mathcal{C})(\delta_g - \delta_e - \Delta_{LS})}{\Delta_{width}^2 + (\delta_g - \delta_e - \Delta_{LS})^2}. \quad (21)$$

Here, the line shape of the CPT resonance as a function of $\delta_g - \delta_e$ is composed of the sum of the symmetric Lorentzian function (first term) and the antisymmetric Lorentzian function (second term), with the linewidth Δ_{width} and the light shift Δ_{LS} . This line shape matches that obtained for the three-level model, except for their amplitudes ($\text{Re}(\mathcal{C})$ and $\text{Im}(\mathcal{C})$). Thus, we are able to derive the line shape, linewidth, and light shift of the CPT resonance for the multi-level atomic model.

In a condition where CPT resonance frequencies are resolved clearly by the magnetic field and the frequencies of the excitation lights are tuned to the excited state $6P_{1/2} F' = 3$ or 4, \mathcal{C} can be replaced by the following simple expressions after certain approximations.

$$\begin{aligned} \mathcal{C} = & -\frac{\gamma_f}{4 \left[\gamma_f^2 + (\Delta_{opt} + \Delta'_{hfs} / 2)^2 \right]} \left[(\rho_{gg} + \rho_{ee}) + i(\rho_{gg} - \rho_{ee}) \frac{\Delta_{opt} + \Delta'_{hfs} / 2}{\gamma_f} \right] \sum_{u=17}^{23} \Omega_{gu} \Omega_{eu}^* \\ & -\frac{\gamma_f}{4 \left[\gamma_f^2 + (\Delta_{opt} - \Delta'_{hfs} / 2)^2 \right]} \left[(\rho_{gg} + \rho_{ee}) + i(\rho_{gg} - \rho_{ee}) \frac{\Delta_{opt} - \Delta'_{hfs} / 2}{\gamma_f} \right] \sum_{u=24}^{32} \Omega_{gu} \Omega_{eu}^* \end{aligned} \quad (22)$$

Note that the term $\Delta_{opt} + \Delta'_{hfs} / 2$ (or $\Delta_{opt} - \Delta'_{hfs} / 2$) is nearly zero when the excitation lights are almost tuned to $F' = 3$ (or 4) levels. When the excitation lights are detuned, asymmetry in the CPT spectrum appears, as reported in [21,26,27]. A rigorous derivation of the CPT spectrum in the 32-level model is presented in the Appendix.

III. EXPERIMENTAL SETUP

The experimental setup is nearly identical to the one described in our previous paper [20]. Magnetic materials are carefully removed from the vicinity of the cell to reduce the inhomogeneous magnetic field and the linewidth of the magnetic-field-sensitive CPT resonance. We utilized several Cs-vapor cells filled with nitrogen buffer gas at room temperature. The buffer gas pressure for each cell was determined from the measured value of the CPT resonance frequency shift based on the reported value of the buffer gas shift [28]. The pressure and shape of these gas cells are

listed in Table I, along with the decay rate of the ground states γ_p and the decay rate of the excited states Γ . γ_p is determined from the CPT resonance linewidth when the excitation light intensity is close to zero. Γ is determined by the fitting with the Voigt function of the absorption spectrum of the monochromatic light when the incident light intensity is close to zero.

IV. RESULTS AND DISCUSSION

A. Dependence of CPT spectrum on buffer-gas pressures

Figures 3 (a)-(c) show the CPT spectra observed in three gas cells with different buffer gas pressures from 0.09 to 11.52 kPa excited by circular polarization tuned to $F'=4$ levels. There are seven Zeeman peaks in each measurement, which correspond to the resonance (m,m) between two ground levels of $|F=3, m_F=m\rangle$ and $|4, m\rangle$ from $m=-3$ to $+3$, respectively. The experimental results show how large the linewidth and the amplitude distribution of the CPT resonance vary with the gas pressure of the cell.

In cells with higher buffer gas pressure, the linewidth of the CPT resonance becomes narrower. As the pressure of the buffer gas in the cell increases, Cs - Cs collisions are suppressed and Cs - N₂ collisions progress, resulting in a decrease in the decay rates of the ground states and an increase in the decay rates of the excited states, respectively. As shown in Eq. (18), they cause a narrowing of the linewidth of the CPT spectrum. As for the amplitude distribution of the CPT spectra, in the high-pressure cell, the CPT resonance of $(-3, -3)$ is more significant, which may suggest that the occupancy among the ground states is different depending on the buffer gas pressure.

Previously, Warren et al. calculated the CPT spectrum of ⁸⁷Rb vapor with 10 Torr (1.3 kPa) Ne buffer gas at room temperature using “the uniform relaxation” represented in Eq. (11) as a source matrix [22]. In a different approach, Matsuda et al. calculated the CPT spectrum of ¹³³Cs vapor with 10 kPa Ne - Ar buffer gas at 80 °C using “the magnetic dipole relaxation” represented in Eq. (12) [23]. The two relaxations are illustrated in Fig. 2. In the present paper, we show that such a difference in the intensity distribution can be explained by a ratio of the combination of the two relaxation processes. Therefore, we assume that the relaxation rate of the ground states γ_p is the sum of

the relaxation rates of the two processes $\gamma_p^{(uni)}$ and $\gamma_p^{(M1)}$, namely, $\gamma_p = \gamma_p^{(uni)} + \gamma_p^{(M1)}$. If we define the ratio of the uniform relaxation to the total relaxation as r , the ratio of the magnetic dipole relaxation is $(1-r)\gamma_p$. Then, the source matrix for the total relaxation process is written as follows.

$$\Lambda_l^{(uni+M1)} = \sum_{m=1, m \neq l}^{16} \left[\frac{1}{15} r + \tilde{T}_{ml}^2 (1-r) \right] \gamma_p \rho_{mm} + \sum_{n=17}^{32} T_{nl}^2 \Gamma \rho_{nn} \quad (23)$$

The values of γ_p and Γ in Table I were determined experimentally from the CPT spectra and the absorption spectra measured for each cell, respectively. Substituting Eq. (23) into Eq. (14), we calculated the Zeeman CPT

spectrum for each cell so as to fit to the experimental results by changing r as a fitting parameter.

Figures 3 (d)-(f) show the calculated CPT spectra for $r = 1.00, 0.60$, and 0.30 for the buffer gas pressures of $0.09, 1.35$, and 11.52 kPa, respectively. Note here that the buffer gas shift, which is clearly seen in Cell3, is not included in the calculation. The three calculated amplitude distributions of the CPT spectrum approximately reproduce those for the corresponding experimental results. We ascertain that the uniform relaxation process is dominant in the cell with gas pressure of 0.09 kPa. We also see that the higher the buffer gas pressure, the closer the ground-state relaxation process becomes to the magnetic dipole relaxation. This is presumably because Cs atoms are less likely to move spatially in a cell with a high buffer gas pressure. Thus, atom collisions and atom replacement, which are features of the uniform relaxation, are less likely to occur in a cell with a high buffer gas pressure.

B. First-order Zeeman CPT spectrum

Here, we discuss how the patterns of the Zeeman CPT spectra are related to the excitation levels ($F' = 3$ or 4) and the polarization scheme of the excitation lights. Blue solid lines in Fig. 4(a) and (b) indicate the CPT spectra observed in Cell2 by excitation with circularly polarized lights $\sigma^- - \sigma^-$ whose frequencies are tuned to $F' = 4$ and $F' = 3$ levels, respectively. In the spectrum excited to $F' = 4$ levels, the $(-3, -3)$ resonance produces the largest signal. In contrast, a roughly antisymmetric pattern is observed in the CPT spectrum excited to $F' = 3$, where the $(0, 0)$ resonance is the largest, and a positive value of m produces a larger signal than a negative value. The calculated spectra for $r = 0.6$ with $\sigma^- - \sigma^-$ excitation tuned to $F' = 4$ and 3 levels, respectively shown in Fig. 4(a) and (b) as red solid lines, are in good agreement with the patterns observed in the experiments. The amplitude of the $(0, 0)$ resonance in the experimental CPT spectrum tuned to $F' = 3$ is normalized to the calculated one. The amplitude values on the vertical axis are relative to the calculated amplitude of the $(0, 0)$ resonance in $\sigma^- - \sigma^-$ excitation tuned to $F' = 3$. The observed $(-3, -3)$ and $(3, 3)$ resonance signals at both ends of the detuning frequency are smaller than the calculated results. This is presumably due to the spatial inhomogeneity of the magnetic field in the experimental system.

The amplitude of the Zeeman CPT spectra is determined by the sum of populations of the ground states related to the CPT resonance, and the product of two Rabi frequencies responsible to the Λ scheme, as shown in Eq. (22). For each resonance signal excited to $F' = 4$ and 3 levels, the former and latter are respectively shown by blue triangles and red stars in Fig. 4(c) and (d). Though the distribution of the sum of the populations is similar regardless of $F' = 4$ and 3 levels, the pattern of the product of Rabi frequencies is different for the two excitations depending on the values of their Clebsch-Gordan coefficients. Here, note that the $(-3, -3)$ resonance excited to $F' = 3$ is observed in both the numerical and experimental results even though the product of the Rabi frequencies is zero, which is due to the contribution from the detuned excitation to $F' = 4$ levels.

We also calculated the Zeeman CPT spectra excited with the $\text{Lin} \perp \text{Lin}$ polarization scheme to $F' = 4$ levels and with the $\text{Lin} \parallel \text{Lin}$ polarization scheme to $F' = 3$ levels, using the same parameters and intensity of the laser for the experiment. in Fig. 4. The results are shown in Fig. 5(a) and (b), respectively, where we find that their patterns are almost identical to those observed experimentally [17, 20]. At $I_1 = I_2 = 6.6 \mu\text{W} / \text{mm}^2$, the amplitude ratio of the $(0, 0)$ CPT resonance excited with the $\text{Lin} \perp \text{Lin}$ polarization to $F' = 4$ levels, with $\sigma^- - \sigma^-$ polarization to $F' = 4$ levels, with $\sigma^- - \sigma^-$ polarization to $F' = 3$ levels, and the sum of the $(-1, 1)$ and $(1, -1)$

resonances excited with the Lin \parallel Lin polarization to $F'=3$ levels is calculated to be 124 : 3.0 : 1: 22. Thus, the Lin \perp Lin polarization scheme produces the largest amplitude of the (0, 0) CPT resonance in the D_1 transition of ^{133}Cs atoms.

C. Second-order Zeeman CPT spectrum

Depending on the strength of the quantized magnetic field, each Zeeman CPT spectrum is split into three Λ -scheme resonances of (m, m) , $(m-1, m+1)$, and $(m+1, m-1)$ due to the second order Zeeman effect. The resonances of $(m-1, m+1)$ and $(m+1, m-1)$ via $m'_F = m$ are created by the excitation scheme of the linear-linear polarization, whereas the (m, m) resonance is created by two σ^+ polarizations via $m'_F = m+1$, or with two σ^- polarizations via $m'_F = m-1$. For such a double- Λ scheme of the (m, m) resonance generated by the linear-linear polarization, Liu *et al.*, derived the condition where a dark state common to the two Λ schemes exists [17], as follows. Here, we define level $|s\rangle$ as $F=3$ and $m_F = m$, $|s'\rangle$ as $F=4$ and $m_F = m$, $|t\rangle$ as $F'=3$ and $m_F = m+1$, $|t'\rangle$ as $F'=3$, and $m_F = m-1$. θ is the angle between two electric fields.

$$e^{2i\theta} = \frac{\Omega_{2s't}^{\sigma+} \Omega_{1st'}^{\sigma-}}{\Omega_{1st}^{\sigma+} \Omega_{2s't'}^{\sigma-}} \quad (24)$$

Conversely, when the dark state for a transition is the bright state for the other transition, the two Λ schemes act to weaken each other. The condition is as follows.

$$e^{2i\theta} = -\frac{\Omega_{1st}^{\sigma+} \Omega_{1st'}^{\sigma-}}{\Omega_{2s't}^{\sigma+} \Omega_{2s't'}^{\sigma-}} \quad (25)$$

In the case of $m=0$ in the D_1 transition of ^{133}Cs , Eq. (24) becomes $e^{2i\theta} = -1$. Therefore, in the Lin \perp Lin (or push-pull) scheme with $\theta = \pi/2$, a common dark state exists and the (0, 0) CPT resonance occurs, along with $(-1, 1)$ and $(1, 1)$ [17]. In contrast, in the Lin \parallel Lin scheme with $\theta = 0$, no (0, 0) CPT resonance occurs, since the dark state for one Λ scheme becomes the bright state for the other (as shown in Fig. 5(d)). Note that in the case of $m \neq 0$, Eq. (25) is still satisfied in the Lin \parallel Lin scheme with $\theta = 0$ and $\mathcal{E}_1 = \mathcal{E}_2$.

We measured the second order Zeeman CPT spectrum in the Lin \parallel Lin scheme in detail. The blue lines in Fig. 6 indicate splitting in the vicinity of the (m, m) resonances for $m = -3, \dots, +3$ excited to $6\text{P}_{1/2}$ $F'=3$ levels with the Lin \parallel Lin polarization. Except for $m=0$, we can clearly observe the (m, m) CPT resonances. The amplitude of the (m, m) CPT resonance increases as the absolute value of m increases. We also calculated the CPT spectrum using the multi-level equations discussed above and found that they agree well the experimental results, as indicated by the yellow lines in Fig. 6. This consistency between the experimental results and the multi-level calculation suggests that an additional condition is required in the double- Λ scheme to suppress the CPT resonance. We explain this as follows.

As written in Eq. (15), a measure of transparency is $\sum_{n=17}^{32} \sum_{l=1}^{16} \text{Im}(\Omega_{nl} \rho_{ln})$. Here, we consider a double- Λ scheme composed of the ground states pair, $|g\rangle$ and $|e\rangle$, and the excited states associated with σ^+ and σ^- polarizations, $|n^+\rangle$ and $|n^-\rangle$. The contribution of this double- Λ scheme to transmittance is given by the following.

$$\begin{aligned} \text{Im}\left(\Omega_{n^+g}\rho_{gn^+} + \Omega_{n^-g}\rho_{gn^-}\right) &= \text{Im}\left[i\Omega_{n^+g}\frac{\sum_{v=17}^{32}\Omega_{gv}\rho_{vn^+} - \sum_{u=1}^{16}\Omega_{un^+}\rho_{gu}}{\Gamma_g + \Gamma_{n^+} + 2i(\delta_g - \delta_{n^+})} + i\Omega_{n^-g}\frac{\sum_{v=17}^{32}\Omega_{gv}\rho_{vn^-} - \sum_{u=1}^{16}\Omega_{un^-}\rho_{gu}}{\Gamma_g + \Gamma_{n^-} + 2i(\delta_g - \delta_{n^-})}\right] \quad (26) \\ &\simeq -\frac{1}{4\gamma_f}\left\{\left(\left|\Omega_{gn^+}\right|^2 + \left|\Omega_{gn^-}\right|^2\right)\rho_{gg} + \text{Re}\left[\left(\Omega_{gn^+}^*\Omega_{en^+} + \Omega_{gn^-}^*\Omega_{en^-}\right)\rho_{ge}\right]\right\} \end{aligned}$$

Here, we assume the frequencies of the excitation lights are tuned to both the n^+ and n^- levels, such that

$|\delta_g - \delta_{n^\pm}| \ll \gamma_f$. Similarly,

$$\text{Im}\left(\Omega_{n^+e}\rho_{en^+} + \Omega_{n^-e}\rho_{en^-}\right) \simeq -\frac{1}{4\gamma_f}\left\{\left(\left|\Omega_{en^+}\right|^2 + \left|\Omega_{en^-}\right|^2\right)\rho_{ee} + \text{Re}\left[\left(\Omega_{gn^+}^*\Omega_{en^+} + \Omega_{gn^-}^*\Omega_{en^-}\right)\rho_{ge}\right]\right\}. \quad (27)$$

The term associated with ρ_{gg} or ρ_{ee} is the contribution of one-photon absorption. From Eqs. (21–22), the term

associated with ρ_{ge} is written as follows.

$$\begin{aligned} \text{Re}\left[\left(\Omega_{gn^+}^*\Omega_{en^+} + \Omega_{gn^-}^*\Omega_{en^-}\right)\rho_{ge}\right] &= \frac{\text{Re}\left[\left(\Omega_{gn^+}^*\Omega_{en^+} + \Omega_{gn^-}^*\Omega_{en^-}\right)\mathcal{C}\right]\Delta_{width}}{\Delta_{width}^2 + (\delta_g - \delta_e - \Delta_{LS})^2} + \frac{\text{Im}\left[\left(\Omega_{gn^+}^*\Omega_{en^+} + \Omega_{gn^-}^*\Omega_{en^-}\right)\mathcal{C}\right](\delta_g - \delta_e - \Delta_{LS})}{\Delta_{width}^2 + (\delta_g - \delta_e - \Delta_{LS})^2} \\ &\simeq -\frac{\rho_{gg} + \rho_{ee}}{4\gamma_f} \frac{\Delta_{width}}{\Delta_{width}^2 + (\delta_g - \delta_e - \Delta_{LS})^2} \left|\Omega_{gn^+}^*\Omega_{en^+} + \Omega_{gn^-}^*\Omega_{en^-}\right|^2 \end{aligned} \quad (28)$$

Therefore, the amplitude of the CPT resonance depends on the square of $\Omega_{gn^+}^*\Omega_{en^+} + \Omega_{gn^-}^*\Omega_{en^-} \equiv \Omega_{1st}^{\sigma+}\Omega_{2s't}^{*\sigma+} + \Omega_{1st'}^{\sigma-}\Omega_{2s't'}^{*\sigma-}$. This value is 0 for $m=0$ but is proportional to 0.0065, 0.021, and 0.027 for $m=\pm 1, \pm 2$, and ± 3 , respectively. Thus, in order to prohibit the (m, m) CPT resonance excited to $F'=3$ levels with the linear-linear polarization in case of the double- Λ scheme, $\sum_{u=17}^{23}\Omega_{gu}\Omega_{eu}^*=0$ is required in addition to the conditions of $\theta=0$ and $\mathcal{E}_1=\mathcal{E}_2$. This condition is equivalent to

$$\Omega_{1st}^{\sigma+}\Omega_{2s't}^{*\sigma+} = -\Omega_{1st'}^{\sigma-}\Omega_{2s't'}^{*\sigma-}. \quad (29)$$

D. Dependence of CPT resonance on excitation intensity

In our previous paper [20], we showed that the amplitude of the $(-1, 1)$ and $(1, -1)$ CPT resonances excited with the $\text{Lin} \parallel \text{Lin}$ polarization increases approximately in proportion to the excitation intensity, while the amplitude of the $(0, 0)$ CPT resonance excited with $\sigma^- - \sigma^-$ polarization moderately saturates. We concluded that the former can be described by the simple three-level model and the latter by the four-level model with a trap state. However, such behaviors should be explained by one complete equation that considers all sublevels related to the D_1 line of ^{133}Cs . In this section, we compare the experimental results of the dependency of the $(-1, 1)$ and the $(0, 0)$ CPT resonances on excitation intensity with the calculated ones using the present multi-level model.

The peak amplitudes of the CPT resonance were measured for Cell2 (N_2 : 1.35 kPa) as a function of the intensity of the excitation lights with $\sigma^- - \sigma^-$ polarization tuned to $F' = 3$ (green dot) and $F' = 4$ (blue rectangle) levels, and with the Lin \parallel Lin polarization tuned to $F' = 3$ (red triangle) and $F' = 4$ (magenta star) levels, as shown in Fig. 7. Similar to our previous results, the amplitude of the CPT resonance excited with $\sigma^- - \sigma^-$ polarization to $F' = 4$ levels saturates, but that excited with Lin \parallel Lin polarization to $F' = 3$ levels increases as the intensity increases and exceeds the former at more than $3 \mu\text{W} / \text{mm}^2$. The solid lines in Fig. 7 show the peak amplitudes calculated for the same experimental conditions using the 32-level model. As we can see, the amplitude calculated for Lin \parallel Lin polarization excited to $F' = 3$ increases in proportion to the intensity of light, and the magnitudes are fitted to the experimental ones. The amplitudes calculated for the other conditions are also consistent with the experimental data, especially for $\sigma^- - \sigma^-$ polarization excited to $F' = 4$ levels. These findings indicate that the amplitude calculated using the multi-level model reproduces the experimental results. However, the linewidths of the calculated CPT spectrum are about twice the length of the experimental linewidth. The dashed line in Fig. 7 shows the amplitude calculated for the Lin \perp Lin polarization scheme excited to $F' = 4$ levels. We can see here that the peak amplitude of CPT resonance at the excitation intensity above $3 \mu\text{W} / \text{mm}^2$ is the largest in the order of the Lin \perp Lin polarization excited to $F' = 4$ levels, the Lin \parallel Lin polarization excited to $F' = 3$ levels, $\sigma^- - \sigma^-$ polarization excited to $F' = 4$ levels, the Lin \parallel Lin polarization excited to $F' = 4$ levels, $\sigma^- - \sigma^-$ polarization excited to $F' = 3$ levels.

To investigate the difference between dependencies on the excitation intensity for $\sigma^- - \sigma^-$ excitation and Lin \parallel Lin excitation, we calculated the population of trap states. State $|8\rangle$ in Fig. 1 is a trap state for the excitation to $F' = 4$ levels, and states $|1\rangle$, $|8\rangle$, and $|9\rangle$ are trap states for the excitation to $F' = 3$ levels. The populations of the trap states for several excitation schemes are shown in Fig. 8 as a function of the excitation intensity. When free from the excitation lights, the ground-state populations are thermally equivalent. For $\sigma^- - \sigma^-$ excitation, the population of the trap state increases as the intensity increases and reaches 80% at more than $3 \mu\text{W} / \text{mm}^2$. In contrast, that for Lin \parallel Lin excitation does not depend on the excitation intensity and is almost constant at 20%. These findings clarify that the CPT amplitude for $\sigma^- - \sigma^-$ excitation saturates while the CPT amplitude for the Lin \parallel Lin excitation increases in proportion to the excitation intensity. The population of the trap state for the Lin \perp Lin excitation to $F' = 4$ levels versus excitation intensity is almost same as that for Lin \parallel Lin excitation to the $F' = 4$ levels.

V. CONCLUSION

We constructed a computational multi-level atomic model of the Liouville density-matrix equation to investigate the CPT resonances excited by the bichromatic lights of various excitation schemes between the ground hyperfine levels. The model contains 32 Zeeman sublevels on the D_1 line of ^{133}Cs atoms. We also derived formulations for the line shape, linewidth, and light shift of the CPT resonance spectrum analytically from the present multi-level atomic model. By calculating the model numerically with the experimentally determined decay rates of the ground and the excited states, the amplitude and shape of the CPT resonance were obtained for different excitations by circular or linear polarization. We confirmed that the calculations accurately reproduced the experimental spectra

observed in Cs vapor cells and elucidated the mechanism underlying various characteristics. Specifically, we found that the Zeeman CPT spectra with different buffer gas pressures vary due to the relaxation process. The amplitude of the first order Zeeman CPT spectra depends on the common detuning frequency of the excitation light. The (m, m) CPT resonance (except for $(0, 0)$) appears in the second order Zeeman CPT spectrum in the $\text{Lin} \parallel \text{Lin}$ excitation, which demonstrates the need for an additional condition to prohibit the CPT resonance. We also clarified that the amplitude for $\sigma^- - \sigma^-$ excitation saturates while that for $\text{Lin} \parallel \text{Lin}$ excitation increases in proportion to the excitation intensity coincident with a variation of the population of the trap state.

These findings indicate that our computational multi-level model can help clarify the phenomena of the CPT resonance and promote the development of miniature atomic clock devices. To further improve the multi-level atomic model, it would be necessary to add spatial characteristics that reflect the Gaussian intensity distribution of the excitation light, the attenuation of light in the thickness direction of the gas cell, and the spatial non-uniformity of the magnetic field.

APPENDIX: CPT spectrum in 32-level model

Here we consider the shape of the CPT spectrum using the 32-level model. First, we introduce shorthand symbols to represent symmetric and asymmetric Lorentz functions, namely, $\mathcal{S}(x, w) = \frac{w}{x^2 + w^2}$ and $\mathcal{A}(x, w) = \frac{x}{x^2 + w^2} = \mathcal{S}(x, w)^* x / w$. We can find $(w \pm ix)^{-1} = \mathcal{S}(x, w) \mp i\mathcal{A}(x, w)$. From the Liouville equation in Eq. (14), for indices $g = 1, \dots, 7$ and $i = 17, \dots, 32$, $\text{Im}(\Omega_{gi}\rho_{ig})$ is written as follows.

$$\text{Im}(\Omega_{gi}\rho_{ig}) = \frac{\mathcal{S}(\delta_i - \delta_g, \gamma_f)}{2} \left[|\Omega_{gi}|^2 (\rho_{gg} - \rho_{ii}) + \text{Re} \left(\sum_{v=8}^{16} \Omega_{vi} \Omega_{ig} \rho_{gv} \right) - \frac{\delta_i - \delta_g}{\gamma_f} \text{Im} \left(\sum_{v=8}^{16} \Omega_{vi} \Omega_{ig} \rho_{gv} \right) \right] \quad (\text{A1})$$

For simplicity, we ignore the coherence between any two magnetic sublevels in the same hyperfine state. In a similar manner, for indices $e = 8, \dots, 16$ and $i = 17, \dots, 32$, $\text{Im}(\Omega_{ei}\rho_{ie})$ is written as follows.

$$\text{Im}(\Omega_{ei}\rho_{ie}) = \frac{\mathcal{S}(\delta_i - \delta_e, \gamma_f)}{2} \left[|\Omega_{ei}|^2 (\rho_{ee} - \rho_{ii}) + \text{Re} \left(\sum_{v=1}^7 \Omega_{ev} \Omega_{iv} \rho_{ve} \right) - \frac{\delta_i - \delta_e}{\gamma_f} \text{Im} \left(\sum_{v=1}^7 \Omega_{ev} \Omega_{iv} \rho_{ve} \right) \right] \quad (\text{A2})$$

Here, we define transmittance T as $T = 1 - \alpha \sum_{n=17}^{32} \sum_{l=1}^{16} \rho_{nl} \text{Im}(\Omega_{ln}\rho_{nl})$, $\alpha = \frac{N_{atom} \hbar \omega \Gamma}{(I_1 + I_2) S_{beam}}$. N_{atom} , $\hbar \omega$, and S_{beam}

are the number of interacting atoms, the energy of a photon of the excitation light, and the cross section of the beam, respectively. Thus, T can be written as

$$T = 1 - \sum_{i'=17}^{32} \sum_{l'=1}^{16} \mathcal{F}_1(l', i') + \sum_{g'=1}^7 \sum_{e'=8}^{16} \mathcal{F}_2(g', e') \quad (\text{A3})$$

$$\mathcal{F}_1(l, i) = \frac{\alpha}{2\Gamma} \mathcal{S}(\delta_i, \gamma_f) |\Omega_{li}|^2 (\rho_{li} - \rho_{ii}), \quad \mathcal{F}_2(g, e) = -\frac{\alpha}{2\Gamma} \sum_{i=17}^{32} \mathcal{S}(\delta_i, \gamma_f) \text{Re} [\Omega_{ei} \Omega_{ig} \rho_{ge}], \quad (\text{A4})$$

where $\mathcal{S}(\delta_i - \delta_g, \gamma_f) \approx \mathcal{S}(\delta_i - \delta_e, \gamma_f)$ is replaced with $\mathcal{S}(\delta_i, \gamma_f)$. We also assume $|\delta_g - \delta_e| \ll \gamma_f$, as this is satisfied in typical situations for CPT resonance measurements. $\mathcal{F}_1(l, i)$ represents the one-photon absorption from $|l\rangle$ to $|i\rangle$. $\mathcal{F}_2(g, e)$ represents the CPT spectrum corresponding to the resonance state of $|g\rangle$ and $|e\rangle$. We now focus on the details of the CPT spectrum, $\mathcal{F}_2(g, e)$. From Eq. (18),

$$-\text{Re}(\Omega_{ig} \Omega_{ei} \rho_{ge}) = \mathcal{S}(\Delta_{ge-LS}, \Delta_{ge-w}) \text{Re}(\mathcal{M}) + \mathcal{A}(\Delta_{ge-LS}, \Delta_{ge-w}) \text{Im}(\mathcal{M}) \quad (\text{A5})$$

$$\mathcal{M} \approx \frac{1}{4} \sum_{u=17}^{32} \mathcal{S}(\delta_u - \gamma_f) \Omega_{ig} \Omega_{ei} \Omega_{gu} \Omega_{ue} \left[\left(1 - i \frac{\delta_u - \delta_e}{\gamma_f} \right) \rho_{ee} + \left(1 + i \frac{\delta_u - \delta_g}{\gamma_f} \right) \rho_{gg} \right] \quad (\text{A6})$$

Here, we denote $\Delta_{ge-LS} = \delta_g - \delta_e - \Delta_{LS}$ and $\Delta_{ge-w} = \Delta_{width}$. In cases of $\sigma - \sigma$, $\text{Lin} \parallel \text{Lin}$, or $\text{Lin} \perp \text{Lin}$ excitations, one of the real or imaginary parts of $\Omega_{ig}\Omega_{ei}$ is zero for any values of $g = 1, \dots, 7$, $e = 8, \dots, 16$, and $i = 17, \dots, 32$, which can be confirmed from Eq. (8). Thus, $\Omega_{ig}\Omega_{ei}\Omega_{gu}\Omega_{ue}$ is a real value.

Since the Zeeman shift is negligibly small relative to the hyperfine splitting between $6P_{1/2} F' = 3$ and 4 levels (Δ'_{hfs} in Fig. 1), we can rewrite $\mathcal{S}(\delta_u, \gamma_f) = \mathcal{S}\left(\delta_{F'=3} = \Delta_{opt} + \frac{\Delta'_{hfs}}{2}, \gamma_f\right)$ for $u = 17, \dots, 23$ and $\mathcal{S}(\delta_u, \gamma_f) = \mathcal{S}\left(\delta_{F'=4} = \Delta_{opt} - \frac{\Delta'_{hfs}}{2}, \gamma_f\right)$ for $u = 24, \dots, 32$. When the excitation lights are tuned closely to either of the $F' = 3$ or 4 levels and $\Delta'_{hfs}^2 \gg \gamma_f^2$ is satisfied, we can assume $\mathcal{S}(\delta_{F'=4}, \gamma_f) \ll \mathcal{S}(\delta_{F'=3}, \gamma_f)$ or $\mathcal{S}(\delta_{F'=3}, \gamma_f) \ll \mathcal{S}(\delta_{F'=4}, \gamma_f)$, respectively. Finally, we obtain the CPT spectrum in the case of excitation to $F' = 3$ and 4 levels ($\mathcal{F}_2^{F'=3}(g, e)$ and $\mathcal{F}_2^{F'=4}(g, e)$, respectively) as follows.

$$\mathcal{F}_2^{F'=3}(g, e) = \frac{\alpha}{8\Gamma} \mathcal{S}(\delta_{F'=3}, \gamma_f)^2 \left| \sum_{i=17}^{23} \Omega_{ig} \Omega_{ei} \right|^2 \left[\mathcal{S}(\Delta_{ge-LS}, \Delta_{ge-w})(\rho_{gg} + \rho_{ee}) + \mathcal{A}(\Delta_{ge-LS}, \Delta_{ge-w}) \frac{\delta_{F'=3}(\rho_{gg} - \rho_{ee}) - \delta_g \rho_{gg} + \delta_e \rho_{ee}}{\gamma_f} \right] \quad (A7)$$

$$\mathcal{F}_2^{F'=4}(g, e) = \frac{\alpha}{8\Gamma} \mathcal{S}(\delta_{F'=4}, \gamma_f)^2 \left| \sum_{i=24}^{32} \Omega_{ig} \Omega_{ei} \right|^2 \left[\mathcal{S}(\Delta_{ge-LS}, \Delta_{ge-w})(\rho_{gg} + \rho_{ee}) + \mathcal{A}(\Delta_{ge-LS}, \Delta_{ge-w}) \frac{\delta_{F'=4}(\rho_{gg} - \rho_{ee}) - \delta_g \rho_{gg} + \delta_e \rho_{ee}}{\gamma_f} \right] \quad (A8)$$

These are written as the sum of one symmetric and one asymmetric Lorentz function, whose linewidth is Δ_{ge-w}

and whose center is Δ_{ge-LS} .

ACKNOWLEDGEMENTS

This study was supported by Innovative Science and Technology Initiative for Security Grant Number JPJ004596, ATLA, Japan. K.M. thanks Dr. Yuichiro Yano of National Institute of Information and Communications Technology, for fruitful discussion.

References

- [1] G. Alzetta, A. Gozzini, M. Moi, and G. Orriols, *Nuovo Cimento B* **36**, 5(1976).
- [2] E. Arimondo, *Prog. Opt.* **35**, 257–354 (1996).
- [3] J. Vanier, *Appl. Phys. B* **81**, 421 (2005).
- [4] N. Cyr, M. Têtu, and M. Breton, *IEEE Trans. Instrum. Meas.* **42**, 640 (1993).
- [5] F. Levi, A. Godone, C. Novero, and J. Vanier, Proceeding of European Frequency and Time Forum, Neuchâtel, Switzerland, 1997, pp. 216–220.
- [6] J. Kitching, S. Knappe, and L. Hollberg, *Appl. Phys. Lett.* **81**, 553 (2002).
- [7] L.-A. Liew, S. Knappe, J. Moreland, H. Robinson, L. Hollberg, and J. Kitching, *Appl. Phys. Lett.* **84**, 2694 (2004).
- [8] S. Knappe, V. Shah, P.D.D. Schwindt, L. Hollberg, and J. Kitching, *Appl. Phys. Lett.* **85**, 1460 (2004).
- [9] J. Kitching, *Appl. Phys. Rev.* **5**, 031302 (2018).
- [10] P. Yun, R. Boudot, and E. de Clercq, *Phys. Rev. Appl.* **19**, 024012 (2023).
- [11] M.A. Hafiz, G. Coget, M. Peterson, C. Rocher, S. Guérandel, T. Zanon-Willette, E. de Clercq, and R. Boudot, *Phys. Rev. Appl.* **9**, 064002 (2018).
- [12] S. Yanagimachi, K. Harasaka, R. Suzuki, M. Suzuki, and S. Goka, *Appl. Phys. Lett.* **116**, 104102 (2020).
- [13] Y.-Y. Jau, E. Miron, A.B. Post, N.N. Kuzma, and W. Happer, *Phys. Rev. Lett.* **93**, 160802 (2004).
- [14] S. V. Kargapoltev, J. Kitching, L. Hollberg, A.V. Taichenachev, V.L. Velichansky, and V.I. Yudin, *Laser Phys. Lett.* **1**, 495 (2004).
- [15] T. Zanon, S. Guérandel, E. de Clercq, D. Holleville, N. Dimarcq, and A. Clairon, *Phys. Rev. Lett.* **94**, 193002 (2005).
- [16] A.V. Taichenachev, V.I. Yudin, V.L. Velichansky, and S.A. Zibrov, *JETP Lett.* **82**, 398 (2005).
- [17] X. Liu, J.-M. Mérolle, S. Guérandel, C. Gorecki, E. de Clercq, and R. Boudot, *Phys. Rev. A* **87**, 013416 (2013).
- [18] E. A. Korsunsky and D. V. Kosachiov, *Phys. Rev. A* **60**, 4996 (1999).
- [19] G. Breit and I.I. Rabi, *Phys. Rev.* **38**, 2082 (1931).
- [20] K. Matsumoto, S. Kagami, A. Kirihara, S. Yanagimachi, T. Ikegami, and A. Morinaga, *Phys. Rev. A* **105**, 023110 (2022).
- [21] A.V. Taichenachev, V.I. Yudin, R. Wynands, M. Stähler, J. Kitching, and L. Hollberg, *Phys. Rev. A* **67**, 033810 (2003).
- [22] Z. Warren, M.S. Shahriar, R. Tripathi, and G.S. Pati, *Metrologia* **54**, 418 (2017).
- [23] K. Matsuda, S. Goka, M. Kajita, and Y. Yano, 2018 IEEE International Frequency Control Symposium (IFCS), Olympic Valley, CA, USA, 2018, pp. 1-3, doi: 10.1109/FCS.2018.8597545 (2018).
- [24] M.S. Shahriar, Y. Wang, S. Krishnamurthy, Y. Tu, G.S. Pati, and S. Tseng, *J. Mod. Opt.* **61**, 351 (2014).
- [25] D.A. Steck, Cesium D Line Data, available online at <http://steck.us/alkalidata> (revision 2.2.1, 21 November 2019).
- [26] S. Knappe, M. Stähler, C. Affolderbach, A.V. Taichenachev, V.I. Yudin, and R. Wynands, *Appl. Phys. B* **76**, 57 (2003).

- [27] J. Ghosh, R. Ghosh, F. Goldfarb, J.-L. Le Gouët, and F. Bretenaker, Phys. Rev. A **80**, 023817 (2009).
- [28] L.-C. Ha, X. Zhang, N. Dao, and K. Richard Overstreet, Phys. Rev. A **103**, 022826 (2021).

TABLE I. The pressure and shape of the gas cells used in the present experiments with the decay rate of the ground states γ_p and the decay rate of the excited states Γ , which are determined experimentally.

Cells	Cell1	Cell2	Cell3
N_2 pressure / kPa	0.09	1.35	11.52
Cross section / mm^2	400	314	400
Shape	Rectangular	Cylindrical	Rectangular
Length / mm	20	20	20
$\gamma_p / 2\pi$ / kHz	24.0	0.10	0.085
$\Gamma / 2\pi$ / MHz	41.3	214	1428

Figure Captions

FIG. 1 (Color online) Hyperfine Zeeman structure of the D_1 line of ^{133}Cs . Values are expressed in the unit of angular frequency. $|1\rangle - |7\rangle$, $|8\rangle - |16\rangle$, $|17\rangle - |23\rangle$, and $|24\rangle - |32\rangle$ are the magnetic sublevels of $6\text{S}_{1/2} F = 3$, $6\text{S}_{1/2} F = 4$, $6\text{P}_{1/2} F' = 3$, and $6\text{P}_{1/2} F' = 4$, respectively, labeled in order of magnetic quantum number m_F from $-F$ to F . ω_g^0 and ω_e^0 are unperturbed energies of $6\text{S}_{1/2} F = 3$ and $6\text{S}_{1/2} F = 4$, respectively. ω_{i0} is the medium energy between the unperturbed energies of $6\text{P}_{1/2} F' = 3$ and $6\text{P}_{1/2} F' = 4$. Δ_{hfs} and Δ'_{hfs} are the hyperfine splitting energies of $6\text{S}_{1/2}$ and $6\text{P}_{1/2}$, respectively. ω_1 and ω_2 are frequencies of the excitation lights in a unit of angular frequency. Δ_R and Δ_{opt} are the Raman detuning and the common detuning, respectively, which are defined in the manuscript. Γ and γ_p are the decay rate of $6\text{P}_{1/2}$ (excited) states and $6\text{S}_{1/2}$ (ground) states, respectively.

FIG. 2 (Color online) Schematic diagrams of the relaxation mechanism between ground levels. (a) The uniform relaxation process. (b) The magnetic dipole relaxation process.

FIG. 3 (Color online) Zeeman CPT spectra excited with circularly polarized lights $\sigma^- - \sigma^-$ tuned to the $F' = 4$ levels at $B = 22.7 \mu\text{T}$ observed in three cells at different N_2 pressures. The excitation intensity is $I_1 = I_2 = 6.6 \mu\text{W} / \text{mm}^2$. Experimental spectra in (a) Cell1; 0.09 kPa, (b) Cell2; 1.35 kPa, and (c) Cell3; 11.52 kPa. Calculated spectra with the corresponding parameters for each gas cell of (d) Cell1, (e) Cell2, and (f) Cell3. r is the ratio of the uniform relaxation to the total relaxation. The decay rates of the ground states γ_p and that of the excited states Γ are listed in Table I.

FIG. 4 (Color online) Zeeman CPT spectra in Cell2 excited with circularly polarized light $\sigma^- - \sigma^-$ at $B = 22.7 \mu\text{T}$. N_2 pressures is 1.35 kPa, and the excitation intensity is $I_1 = I_2 = 6.6 \mu\text{W} / \text{mm}^2$. Experimental (blue line) and calculated (red line) CPT spectra with $r = 0.6$ tuned to (a) $F' = 4$ and (b) $F' = 3$ levels. The amplitude of the experimental CPT spectrum is normalized to the calculated (0, 0) CPT resonance tuned to $F' = 3$ levels. The population of two ground states (blue triangle) and the product of Rabi frequencies (red star) for the CPT resonance tuned to (c) $F' = 4$ and (d) $F' = 3$ levels.

FIG. 5 (Color online) Calculated Zeeman CPT spectra excited with (a) Lin \perp Lin scheme tuned to $F' = 4$ levels and with (b) Lin \parallel Lin schemes tuned to $F' = 3$ levels at $B = 22.7 \mu\text{T}$. The excitation intensity is $I_1 = I_2 = 6.6 \mu\text{W} / \text{mm}^2$ and $r = 0.6$.

FIG. 6 (Color online) Calculated (red line) and experimental (blue line) CPT spectra in Cell2 near the (m,m) resonance for $m = -3, \dots, +3$, by $\text{Lin} \parallel \text{Lin}$ excitation tuned to $F' = 3$ levels at $B = 285 \mu\text{T}$. The excitation intensity is $I_1 = I_2 = 1.2 \mu\text{W} / \text{mm}^2$.

FIG. 7 (Color online) Measured (dot) and calculated (line) amplitudes of the $(0, 0)$ or $(-1, 1)$ CPT resonance for different polarization and excitation levels as a function of the excitation intensity I at $B = 139 \mu\text{T}$. N_2 pressures is 1.35 kPa . Calculations are executed with $r = 0.6$, $\Gamma / 2\pi = 214 \text{ MHz}$, and $\gamma_p / 2\pi = 0.10 \text{ kHz}$.

Dashed line is the calculation with $\text{Lin} \perp \text{Lin}$ polarization scheme excited to $F' = 4$ levels. Blue: $\sigma^- - \sigma^-$ polarization excited to $F' = 4$ levels, red: $\text{Lin} \parallel \text{Lin}$ polarization excited to $F' = 3$ levels, green: $\sigma^- - \sigma^-$ polarization excited to $F' = 3$ levels, and magenta: $\text{Lin} \parallel \text{Lin}$ polarization excited to $F' = 4$ levels. Red line is fitted to the red triangle.

FIG. 8 (Color online) The calculated population of trap states for several excitation schemes as a function of excitation intensity. Blue: $\sigma^- - \sigma^-$ polarization excited to $F' = 4$ levels, green: $\sigma^- - \sigma^-$ polarization excited to $F' = 3$ levels, red: $\text{Lin} \parallel \text{Lin}$ polarization excited to $F' = 3$ levels, and magenta: $\text{Lin} \parallel \text{Lin}$ polarization excited to $F' = 4$ levels. Calculations are executed with $r = 0.6$, $\Gamma / 2\pi = 214 \text{ MHz}$, and $\gamma_p / 2\pi = 0.10 \text{ kHz}$ at $B = 139 \mu\text{T}$.

FIG. 1

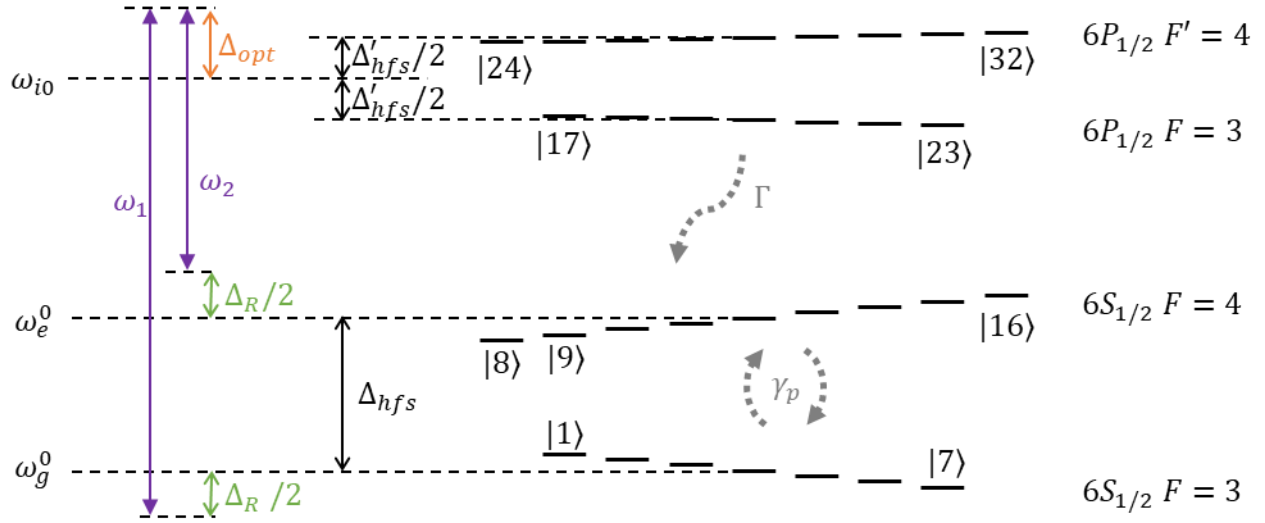


FIG. 2

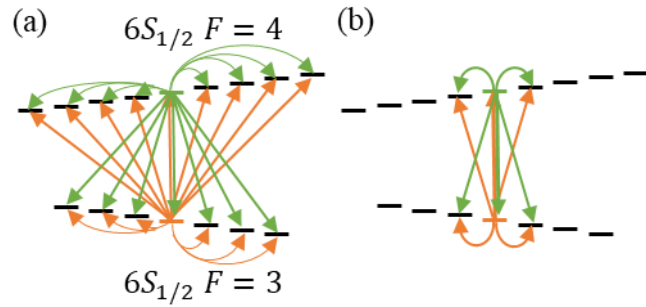


FIG. 3

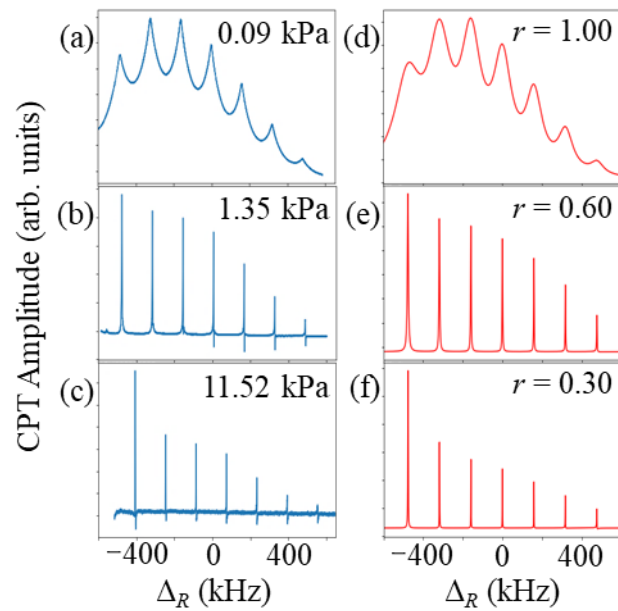


FIG. 4

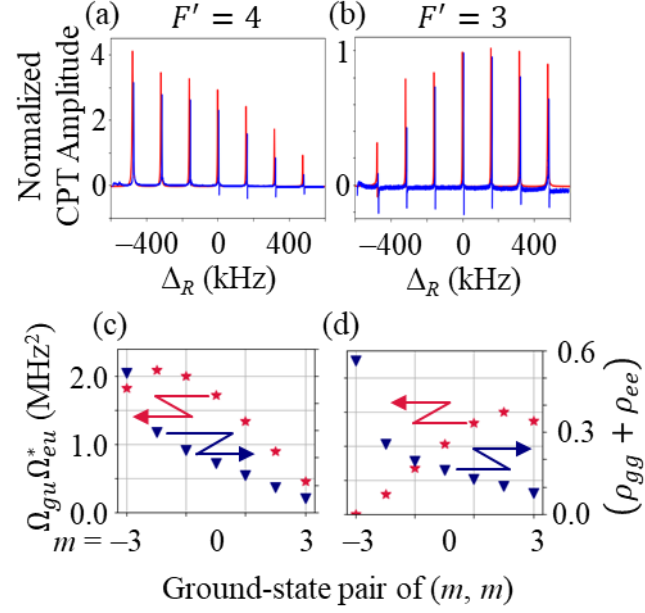


FIG. 5

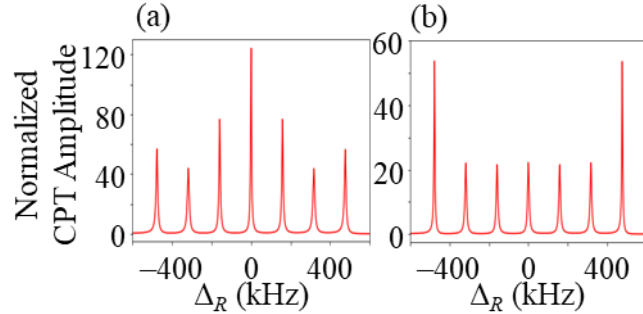


FIG. 6

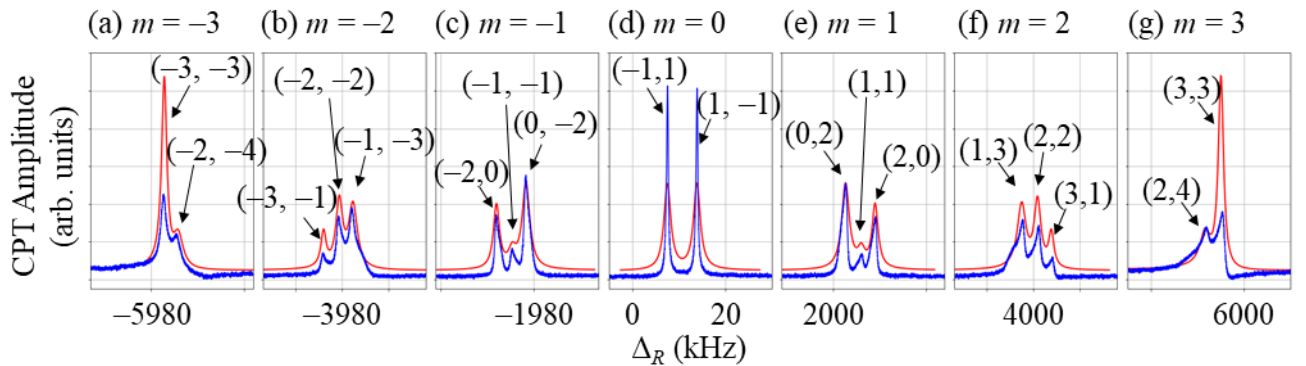


FIG. 7

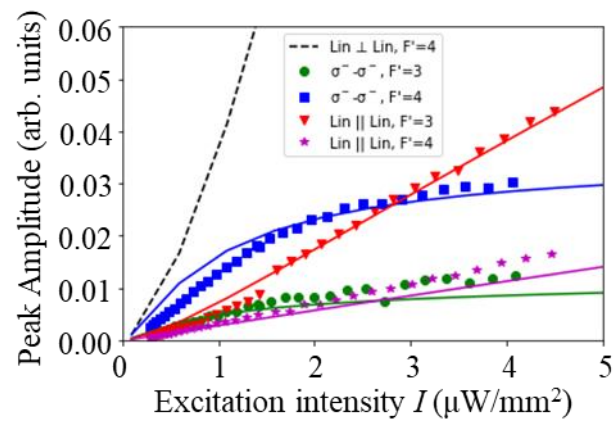


FIG. 8

